A Novel Ultra-Compact Resonator for Superconducting Thin-Film Filters

H. R. Yi, *Senior Member, IEEE*, Stephen K. Remillard, *Member, IEEE*, and Amr Abdelmonem, *Senior Member, IEEE*

Abstract—This paper proposes a novel thin-film resonator structure, which combines the microstrip resonator and the coplanar resonator to form an integrated resonator. This resonator structure has an extremely compact size, as compared to the thin-film resonator structures from the literature, and its resonant frequency was shown theoretically to be less sensitive to, or even insensitive to, the thickness of the substrate. An eight-pole quasi-elliptic filter based on this novel resonator was designed. The exact filter layout was simulated and optimized by full-wave electromagnetic simulation using IE3D software. The full-wave simulated filter response was in good agreement with the theoretical filter response. A filter was fabricated on a double-sided $YBa_2Cu_3O_7$ thin film epitaxially grown on a 2-in-diameter MgO wafer. The measured filter response showed a bandwidth of 1.5 MHz and a center frequency of 850.3 MHz at 78 K. The insertion loss at the passband center was 1 dB, corresponding to a filter Q of 28 000. Steep rejection slopes were obtained at the band edges and rejections reached over 70 dB in approximately 300 kHz from the passband edges. No pronounced changes were observed for input power levels between -20–0 dBm, indicating a relatively high power-handling capability of the filter.

Index Terms—Elliptic filters, microstrip resonators, microwave filters, thin-film resonators.

I. INTRODUCTION

HIGH-PERFORMANCE superconducting filter subsystems based on high-temperature superconducting (HTS) thick- and thin-film technologies have been developed for mobile and satellite communication applications [1]–[3]. The extremely low loss from a high-temperature superconductor offers a unique opportunity for the performance enhancement through higher filter order and reduction of device size through lower loss. For filters based on thin-film technology, substantial effort has been devoted for the miniaturization of the distributed element resonator structures. In an early design, Zhang *et al.* [4] designed a 19-pole bandpass filter with a center frequency of 900 MHz and a bandwidth of 25 MHz using 75-mm-diameter $YBa_2Cu_3O_7$ (YBCO) thin film on a 0.5-mm-thick $LaAlO_3$ substrate. They used a half-wavelength microstrip resonator,
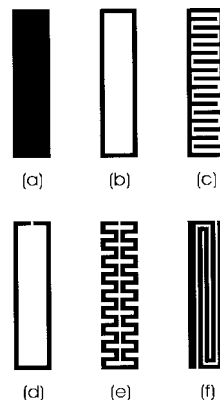

Fig. 1. (a) Half-wavelength microstrip resonator. (b) Loop resonator. (c) Capacitively loaded loop resonator. (d) Open-loop resonator. (e) Meander open-loop resonator. (f) Folded open-loop resonator.

as schematically shown in Fig. 1(a), for their filter design. By removing the central portion of the microstrip, it forms a loop resonator, as shown in Fig. 1(b). However, the frequency reduction is very small for the loop resonator. Lancaster *et al.* [5] reported a capacitively loaded loop resonator, as depicted in Fig. 1(c). The frequency reduction for this resonator is still small. By opening the loop in Fig. 1(b), it forms an open-loop resonator (hairpin), as shown in Fig. 1(d). A big frequency reduction was obtained for this resonator and Hong and Lancaster [6] designed cross-coupled filters with this type of resonator. For the open-loop resonator, one can further reduce the frequency by making the open loop in a meander shape [7], as shown in Fig. 1(e), or fold the open loop to form a folded open-loop resonator [8], as shown in Fig. 1(f).

Besides the miniaturization of the resonator, another issue for superconducting thin-film filters is the thickness variation of the dielectric substrate. The usual tolerance for a 0.5-mm-thick substrate is approximately 10 μm, and sometimes it may even reach 20 μm. The thickness variation of the substrate influences the resonant frequency and the coupling coefficient between the resonators. Consequently, the measured filter response and center frequency without tuning may deviate appreciably from the designed one. Sometimes the filter requires a substantial amount of tuning and even additional iteration to meet the desired operation. In this paper, we report on a novel thin-film resonator that has an extremely compact size for superconducting thin-film filters, while the resonant frequency of the resonator does not change with the substrate thickness for a
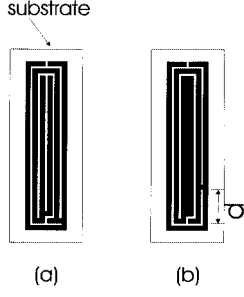
Fig. 2. (a) Shunted open-loop resonator. (b) Modified shunted open-loop resonator.

certain thickness variation of the substrate, as determined by computer simulation using Sonnet software.[1]

II. NOVEL RESONATOR

The velocity of the electromagnetic (EM) wave in a microstrip is given by $v_p = (c/\sqrt{\varepsilon_e})$, where c is the velocity of light in free space and ε_e is the effective dielectric constant. The effective dielectric constant can be approximated [9] by $\varepsilon_e \approx (1/2 + \varepsilon_r/2) + (\varepsilon_r/2 - 1/2)(1 + 12(t_{\mathrm{sub}}/w))^{-1/2}$, where ε_r is the dielectric constant of the substrate, t_{sub} is the thickness of the substrate, and w is the width of the microstrip. When t_{sub} increases, ε_e decreases, and v_p increases. Thus, the resonant frequency for a microstrip resonator increases with increasing substrate thickness. Now consider coplanar lines, the stray capacitance between two microstrips increases when t_{sub} increases. Consequently, the resonant frequency of a coplanar resonator decreases with increasing substrate thickness. Therefore, if one makes a resonator design, which combines a microstrip resonator to a coplanar resonator, it is possible to obtain a stable resonant frequency when the substrate thickness changes within a certain range.

Fig. 2(a) shows a resonator structure that consists of three open loops. The openings of the second open loop (middle one) is in the opposite side to that of the first (outermost) and third open loops. A short circuit (shunt) is introduced between the first and second open loops and between the second and third open loops, respectively. The linewidth of the conducting strip is 0.2 mm. The gap between the strips is 0.1 mm. The outer dimension of this resonator is 1.7 mm × 7 mm. The simulated resonant frequency (f_0) for this resonator is 1768.100 MHz when the substrate thickness is 0.5 mm. When the substrate thickness is increased to 0.51 mm, the resonant frequency (f_a) becomes 1767.853 MHz. The decreasing resonant frequency with increasing substrate thickness is an indication that the coplanar structures influences more on the resonant frequency than the microstrips. Therefore, it is necessary to reduce the coplanar structure. Fig. 2(b) shows a modified design. The third open loop is replaced by a filled microstrip. The shunting position (d) of the short circuit between the first and second open loops is also adjusted.

The circles in Fig. 3(a) are the simulated resonant frequency (f_0) as a function of the shunting position d in Fig. 2(b) for
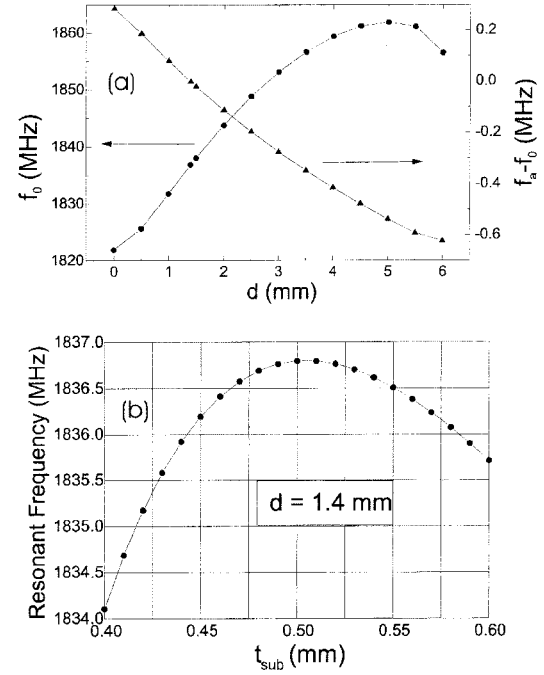
Fig. 3. Circles are the simulated resonant frequencies: (a) as a function of d, the shunting when $t_{\mathrm{sub}} = 0.5$ mm and (b) as a function of t_{sub} when $d = 1.4$ mm. Here, d is the shunting position between the first and second open loops, as shown in Fig. 2. Triangles in (a) are the differences of the resonant frequency ($f_a - f_0$) when t_{sub} is changed from 0.5 to 0.51 mm.

t_{sub} of 0.5 mm. We also simulated the resonant frequency (f_a) for t_{sub} of 0.51 mm, and the difference of f_a and f_0 is shown as triangles in Fig. 3(a). The resonant frequency changes when d changes, as do the portions of contribution from the coplanar structure and microstrip to the frequency. At a shunting position $d = 1.4$ mm, the same resonant frequency is obtained for $t_{\mathrm{sub}} = 0.5$ mm and $t_{\mathrm{sub}} = 0.51$ mm, i.e., $f_0 = f_a$. We would like to mention that, by changing the shunting position between the second and inner microstrip, the resonant frequency will also change. The dependence is not detailed here. In Fig. 3(b), the resonant frequency is simulated for different t_{sub} when $d = 1.4$ mm. A relatively small change of resonant frequency is observed for t_{sub} of approximately 0.5 mm.

To give the reader a comparison of their resonant frequencies for the resonators in Figs. 1 and 2(a), we performed full-wave EM simulation using Sonnet software. In the simulation, all the resonators are set to be of the same size (7 mm × 1.7 mm) and are structured on the same substrate, i.e., 0.5-mm-thick MgO with permittivity of 9.6. The smallest linewidth of the superconducting strip is 0.2 mm, and the smallest space between strips is 0.1 mm. Table I summarizes the simulated results. For the microstrip resonator, the resonant frequency is 7539 MHz. The loop resonator reduces the resonant frequency very slightly to 7330 MHz. The capacitively loaded loop resonator only reduces the resonant frequency to 6429 MHz, which is 83.3% to that of the microstrip resonator. The open-loop resonator significantly reduces the resonant frequency to 3810 MHz, a frequency reduction of approximately 50%. By making the open-loop resonator in a meander shape, the resonant frequency

TABLE I
SIMULATED RESONANT FREQUENCY AND COUPLING COFFICIENT AT 1-mm SEPARATION FOR RESONATORS IN FIG. 1 AND FIG. 2(a). THE RESONATORS ARE
ALL OF THE SAME SIZE 7 mm × 1.7 mm ON 0.5-mm-THICK MgO SUBSTRATE. THE SMALLEST LINEWIDTH OF THE CONDUCTING
STRIP IS 0.2 mm AND THE SMALLEST SPACE BETWEEN STRIPS IS 0.1 mm

Resonator Type	Resonant Frequency (MHz)	Percentage to that of Microstrip	Coupling Coefficient at 1-mm Separation
Microstrip resonator (Fig. 1(a))	7539	100 %	0.065
Loop resonator (Fig. 1 (b))	7330	97.2 %	0.054
Capacitively loaded loop resonator (Fig. 1(c))	6429	85.3 %	0.053
Open loop resonator (Fig. 1(d))	3810	50.5 %	0.012
Meander open loop resonator (Fig. 1(e))	2473	32.8 %	0.00049
Folded open loop resonator (Fig. 1(f))	1932	25.6 %	0.0066
Shunted open loop resonator (Fig. 2(a)	1768	23.5 %	0.0069

is further reduced to 2473 MHz, which is 32.8% to that of the microstrip resonator. However, the biggest reduction of resonant frequency is achieved in the folded open-loop resonator (1932 MHz) and the shunted open-loop resonator (1768 MHz), whose resonant frequencies are just about a quarter of that of the microstrip resonator.

Besides the reduction of the resonator size itself, another key factor for the miniaturization of the overall filter size is to minimize the coupling coefficient between resonators. In Table I, we also showed the simulated coupling coefficient for each pair of coupled resonators with a gap distance of 1 mm. For two resonators with identical resonant frequency of f_0, two split resonant frequencies (f_L and f_H) will be observed in the full-wave EM simulation when they are coupled together. The coupling coefficient is calculated by [6] $k = ((f_H^2 - f_L^2)/(f_H^2 + f_L^2)) \approx (f_H - f_L)/f_0$. The meander open-loop resonator has an extremely small coupling coefficient (0.00049). This is possibly because a large portion of the meander line is in the horizontal direction, and the RF current flowing along the horizontal direction does not couple to the other resonator. Both the folded and shunted open-loop resonators provide very weak coupling coefficient as compared to other resonators, except the meander open-loop resonator. Therefore, very compact filters may be designed using these two types of resonators.

Below we report on the design and experiment of a quasi-elliptic bandpass filter with very narrow bandwidth based on our novel ultra-compact resonator.

III. FILTER DESIGN

A practical resonator structure for designing cellular A-prime band filter (passband 845–846.5 MHz) based on the principle of a shunted open-loop resonator is shown in Fig. 4(a). All the bends are in chamfered shape. The linewidth of the microstrip is 0.254 mm, i.e., 10 mil, and the distance between the microstrips is 0.127 mm. The opening of the outmost loop is protruded to a distance L, which makes it easier for the realization of cross coupling between nonadjacent resonators. The overall dimension of the resonator is 2.16 mm × 17.17 mm.
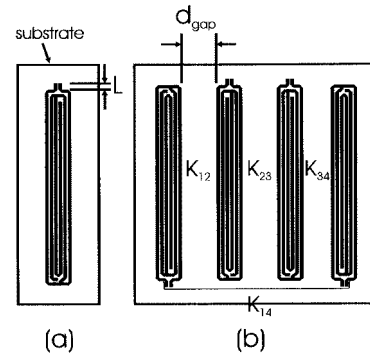

Fig. 4. (a) Shunted open-loop resonator. (b) A quadruplet formed by four resonators, note the coupling configuration between resonators 1 and 2, i.e., K_{12}, and that between resonators 2 and 3, i.e., K_{23} are different, the cross coupling between resonators 1 and 4, i.e., K_{14}, is provided by a thin inductive line.

A cross-coupling technique has been used for producing transmission zeros near the band edge for very sharp rejection slope [10], [11]. Among the cross-coupled filters, a subclass is the so-called cascaded quadruplet (CQ) filter, where the element block (quadruplet) is made up of four resonators having couplings with their neighbors. The CQ structure possesses the significant advantage that each CQ section is entirely responsible for producing one pair of transmission zeros having some kind of symmetry about the passband center [12]. In our filter design, we constructed a quadruplet using four resonators, as shown in Fig. 4(b). Here, we number these four resonators as 1–4 from left to right. For the coupling between resonators 1 and 2, resonator 2 is rotated 180° with respect to resonator 1. For the coupling between resonators 2 and 3, resonator 3 is the mirror of resonator 2. A coupling microstrip provides the cross coupling between resonators 1 and 4. The strength of cross coupling is determined by the length of L, the gap between the coupling microstrip and the resonators, and the linewidth of the coupling microstrip. In Fig. 4(b), L equals 0.508 mm, the gap distance is 50.8 μm, and the linewidth of the coupling microstrip is 76.2 μm.
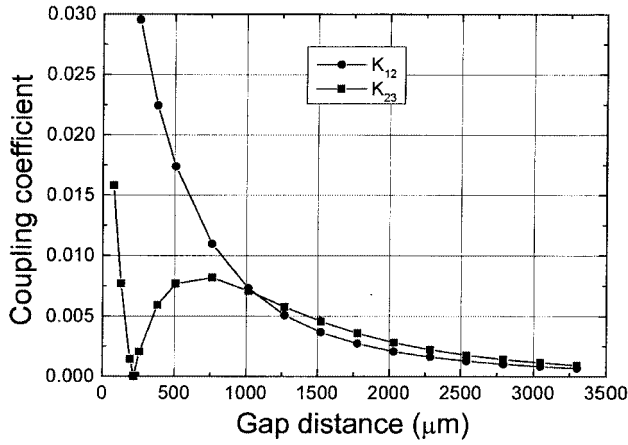
Fig. 5. Simulated coupling coefficient as a function of the gap distance between the resonators. The circles are for the K_{12} coupling configuration and the squares are for the K_{23} coupling configuration in Fig. 4(b).

The coupling coefficient between two resonators is estimated by full-wave EM simulation using IE3D software.[2] For the simulation, the substrate is MgO with a thickness of 0.508 mm, loss tangent of 5×10^{-6}, and permittivity of 9.8. Note that the actual permittivity of MgO is approximately 9.6 at 77 K. A slightly higher value of permittivity in simulation gives a higher center frequency in the measurement, which makes it possible to tune the filter response using dielectric screws. The thickness of the metallic strip is 500 nm and its conductivity is 1.2×10^{13} S/m. Fig. 5 shows the simulated coupling coefficients of K_{12} and K_{23} as a function of the gap distance between the resonators. As can be seen from the figure, K_{12} (circles) decreases monotonically with the increasing gap distance. However, K_{23} (squares) does not vary monotonically with the increasing gap distance. At a gap distance of 216 μm, i.e., 8.5 mil, a zero value of K_{23} is reached. This is an indication that both the electric and magnetic couplings cancel each other out in the K_{23} coupling configuration. Since the electric coupling decays faster than the magnetic coupling against the spacing [13], the electric coupling is dominant for a gap distance of less than 216 μm, and the magnetic coupling is dominant for greater distances. Actually, the sign of the coupling coefficient can be identified by checking the phase relationship of S_{21}, as described in detail in [13]. We have determined that both K_{12} and K_{14} coupling configurations are of electric nature, i.e., negative coupling.

For the quadruplet in Fig. 4(b), we have negative K_{12}, K_{34}, and K_{14}. K_{23} can be selected to have a positive sign by separating resonators 2 and 3 of more than 216 μm apart so that the condition of K_{14} and K_{23} having opposite signs to produce a pair of transmission zeros is satisfied. Note that, for a certain K_{23} value, we have two choices for the gap distance.

Fig. 6 shows a lumped-element circuit model of an eight-pole CQ filter. For this circuit, K_{12}, K_{34}, K_{56}, K_{78}, K_{14}, and K_{58} are of negative sign (electric or capacitive coupling), while K_{23}, K_{45}, and K_{67} are of positive sign (magnetic or inductive coupling). Fig. 7 shows the simulated theoretical response of an eight-pole filter with a passband from 845 to 846.5 MHz. The return loss in the passband is over 24 dB. Two identical pairs
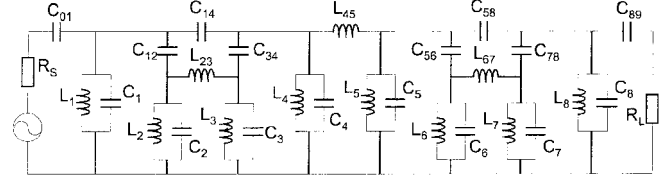
Fig. 6. Lumped-element circuit of an eight-pole filter consisting of two CQs.
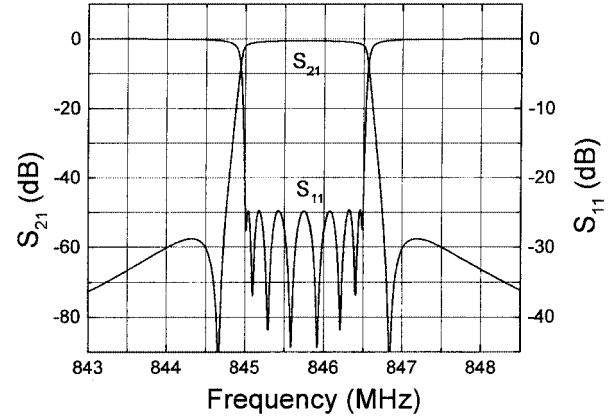

Fig. 7. Theoretical response of an eight-pole CQ filter. The passband is from 845 to 846.5 MHz.
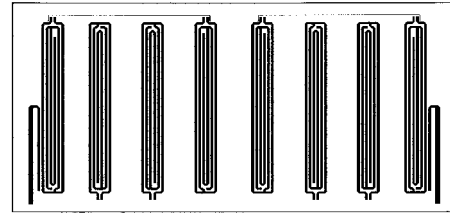

Fig. 8. Layout of an eight-pole thin-film filter on the MgO substrate. The overall chip size is 42 mm $\times$ 20 mm.

of transmission zeros are present at 844.66 and 846.84 MHz. The external Q for the input and output couplings is 499. The coupling coefficients $K_{12} = K_{78} = -1.52 \times 10^{-3}$, $K_{23} = K_{67} = 1.298 \times 10^{-3}$, $K_{34} = K_{56} = -9.071 \times 10^{-4}$, $K_{45} = 9.528 \times 10^{-4}$, and $K_{14} = K_{58} = -3.63 \times 10^{-4}$.

Combining IE3D software and Eagleware software,[3] we have developed a method of constructing and tuning filters of up to 24 poles by full-wave EM simulation. The frequency of each resonator was tuned based on the simulated response. Fig. 8 shows a layout of an eight-pole CQ filter constructed and tuned based on the theoretical response of Fig. 7. The substrate is MgO and the chip size is 42 mm $\times$ 20 mm. This chip size is based on the microstrip linewidth of 254 μm for the resonators. When a smaller microstrip linewidth is used, e.g., 152.4 μm, the chip size can be made considerably smaller. Fig. 9 is the full-wave EM simulated response of this filter layout using IE3D software. As a comparison, the theoretical curves from Fig. 7 are also redrawn here as full curves. Compare this full-wave EM simulated response with the theoretical response, the passband responses are very similar. The EM simulated return loss is 23 dB, only slightly worse than the theoretical return loss of 24 dB. However, the out-band response of S_{21} differs appreciably with the
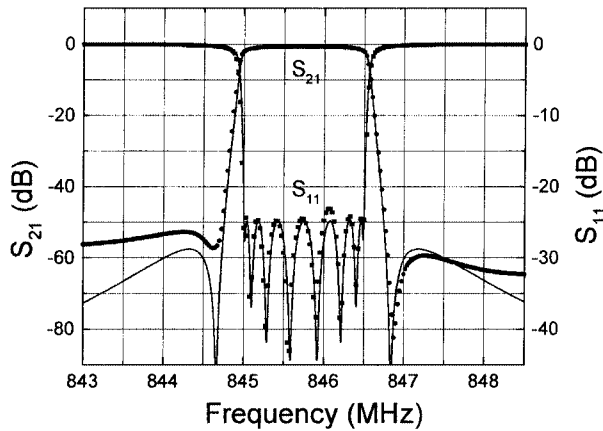
Fig. 9. Simulated S_{11} (squares) and S_{21} (circles) for the layout in Fig. 8 by full-wave IE3D software. Full curves are the theoretical responses. The passband is from 845 to 846.5 MHz.

Fig. 10. Prototype narrow-band filter. The cover was removed from the housing and turned upside down.

theoretical curve in Fig. 7. This is because IE3D software cannot simulate the out-of-band response accurately and correctly [14]. As will be shown by our experimental results in Section IV, the measured out-band response of S_{21} follows more to the theoretical curve rather than to the full-wave EM simulated curve using IE3D. This is an indication that the lack of agreement between the full-wave simulation and the theoretical response is due to IE3D, though the theoretical model in Fig. 6 is so simplified that some existing couplings have not been taken into account.

IV. EXPERIMENT

A chrome mask set consisting of a first mask for defining the filter structure and a second mask for making the contact pads for the input and output was generated based on the layout simulated by IE3D software. A double-sided thermal co-evaporated YBCO film [15] on a 2-in-diameter MgO wafer was used for the fabrication of thin-film filters. The thickness of the MgO wafer was 0.508 mm, and the thickness of the YBCO film on both sides was approximately 700 nm. The backside YBCO was *in situ* coated with a gold layer of approximately 100 nm in thickness. The critical temperature of the YBCO film was higher than 87 K and the critical current density was higher than 2×10^6 A/cm^2 at 77 K. The surface resistance of the film was approximately 0.5 mΩ at 10 GHz and 77 K.

Standard photolithography and ion-beam milling process were used for the filter patterning. After patterning, a photoresist liftoff mask was prepared on the patterned YBCO film. A gold layer of approximately 1-μm thickness was evaporated by an electron gun through the liftoff mask, which, after liftoff, in an acetone ultrasonic bath, formed the contact pads for the input and output ports. A gold layer of approximately 3-μm thickness was then sputtered on top of the backside *in situ* gold. Finally, the patterned wafer was annealed in flowing oxygen at 500 °C for 1 h. After dicing the wafer with a diamond saw, the cleaned filter chip was soldered to a carrier, which was made from Ti-6Al-4V with Ni flash and coated with 5-μm–thick gold, in an in-house developed vacuum glove-box method. The carrier was then screwed in a filter housing, and ultrasonic bonded gold wires were used to connect the input subminiature A (SMA) connector and input microstrip, and the output SMA
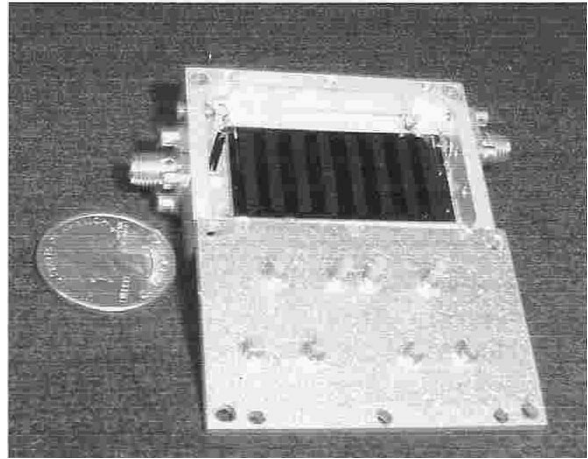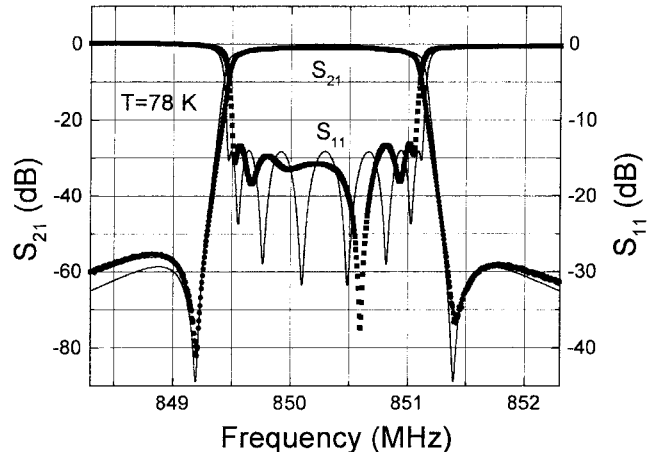

Fig. 11. Measured S_{21} (circles) and S_{11} (squares) of the eight-pole filter in Fig. 10 at 78 K. The full curves are the theoretical responses with external Q of 718 for the input and output couplings.

connector and output microstrip. Finally, the filter housing was sealed by a cover, on which dielectric tuning screws were provided at the appropriate positions for tuning the filter response. The complete package of a prototype narrow-band filter and the cover is shown in Fig. 10.

Fig. 11 shows the measured S_{21} (circles) and S_{11} (squares) of the prototype narrow-band filter in liquid nitrogen with the temperature on the filter housing of approximately 78 K. The full curves correspond to the theoretical responses with an external Q of 718 for both input and output ports. The measurement was taken with an HP 8753D Network Analyzer, and the loss from the cables was subtracted by performing a full two-port calibration using HP 85033D 3.5-mm calibration kits. The bandwidth is 1.5 MHz and the center frequency is 850.3 MHz. The return loss in the passband is over 13.5 dB. Note that the return loss can be improved by improving the design of the input and output. There is a considerable mismatch between the SMA connectors and the input and output microstrips, as this filter was our first designed filter. After improving the input and output microstrips, the return loss has been increased to over 23 dB, as reported in [16]. We would also like to mention that the tuning of the filter reported in [16] takes less than 10 min after it has
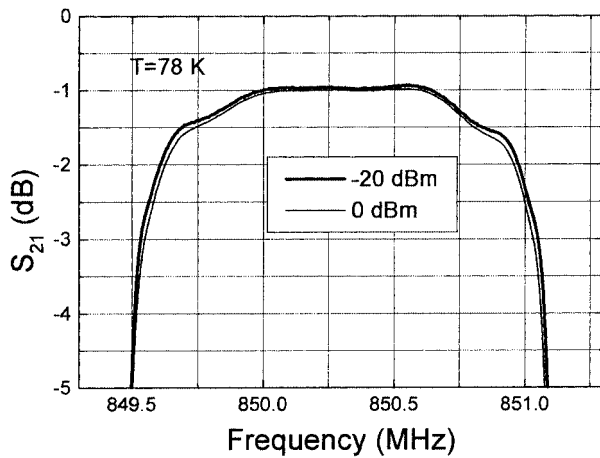
Fig. 12. Insertion loss measured with input power levels at −20 (thick line) and 0 dBm (thin line).

been cooled down in the liquid nitrogen. The insertion loss at the passband center is 1 dB, which corresponds to a filter Q of approximately 28 000. The fly-back values in the S_{21} curve are 56 and 58 dB at the lower and upper frequency sides, respectively. These values are relatively closer to the theoretical value rather than to the full-wave EM simulated values of 53 and 60 dB at the lower and upper frequency sides, as shown in Fig. 9. Steep rejection slopes at the band edges are obtained and rejections reach over 70 dB in approximately 300 kHz from the lower and upper passband edges. Fig. 12 shows the insertion loss measured at 78 K with two different input power levels. The thick line is for −20-dBm input power, and the thin line is for 0-dBm input power. There are no pronounced changes between these two input power levels, indicating a relatively high power-handling capability of the filter.

Since the resonator used in the realized filter has a smaller footprint than previously used resonators, it is important to characterize the filter nonlinearity and verify that it remains acceptable for use in a wireless system. Higher intermodulation distortion (IMD) is expected in smaller filters due to the higher RF current density. It is common to speak about the third-order intercept (IP3) of HTS filters, although, for two reasons, this is not a very useful piece of information. First, the slope of the IMD versus input power is usually less than 3 : 1, preventing accurate extrapolation of IMD to other powers. Second, a filter used in a wireless receiver is the first item in the RF chain (besides cables and connectors) and is followed immediately by an active low-noise amplifier (LNA). By virtue of having gain, the IMD of the LNA controls the IMD of the receiver chain. For example, from circuit theory, if the filter has IP3 of +10 dBm and the LNA (which might be cascaded gain stages) has an output IP3 of +25 dBm and a gain of 40 dB, the resulting output IP3 is +24.986 dBm.

Filter IMD can degrade a wireless system in the event that there are two out-of-band carriers, such as from the transmitter, incident on the filter. This is the condition under which we test HTS filters. The results and explanation of their importance have been reported elsewhere [17]. At 72.5 K, when two A-band transmit carriers (at 874.8 and 875.3 MHz) are incident on the filter at a realistic level of +10 dBm with an in-band carrier at −40 dBm, the resulting in-band IMD is −123.5 dBm, which is

below the approximately −117-dBm sensitivity level of a code-division multiple-access (CDMA) receiver. Typical in-band received power is less than −70 dBm so system degradation from IMD is not expected. The measured IMD was curiously 30 dB lower than that measured on a 7.5-MHz-wide filter in the same frequency range with larger footprint resonators, but using a $Tl_2Ba_2CaCu_2O_8$ superconducting thin film.

V. Conclusion

We have proposed an ultra-compact thin-film resonator structure, which combines the microstrip and coplanar resonators. The resonant frequency was shown theoretically to be less sensitive to, or even insensitive to, the thickness of the substrate, because a variation in the thickness of the substrate has an opposite effect on the self-loading of the resonator than it has on the loading of the resonator to ground. We designed and realized an eight-pole CQ filter based on this novel resonator. The exact filter layout was simulated and optimized by full-wave EM simulation using IE3D software. The full-wave simulated filter response was in good agreement with the theoretical filter response. A prototype filter was fabricated on a double-sided YBCO film epitaxially grown on a 2-in-diameter MgO wafer. The measured filter response showed a bandwidth of 1.5 MHz and a center frequency of 850.3 MHz at 78 K. The insertion loss at the passband center was 1 dB, corresponding to a filter Q of 28 000. Steep rejection slopes at the band edges were obtained and rejections reached over 70 dB in approximately 300 kHz from the lower and upper passband edges. No pronounced changes were observed for incident power levels between −20–0 dBm, indicating a relatively high power-handling capability of the filter.

References

[1] S. K. Remillard, A. Abdelmonem, P. O. Radzikowski, N. D. Lazzaro, and D. S. Applegate, "Field deployable microwave filters made from superconductive thick films," *J. Superconduct.*, vol. 14, pp. 47–56, Jan. 2001.

[2] B. A. Willemsen, "HTS filter subsystems for wireless telecommunications," *IEEE Trans. Applied Superconduct.*, vol. 11, pp. 60–67, Mar. 2001.

[3] R. R. Mansour, S. Ye, B. Jolley, G. Thomson, S. F. Peik, T. Romano, W. C. Tang, C. M. Kudsia, T. Nast, B. Williams, D. Frank, D. Enlow, G. Silverman, J. Soroga, C. Wilker, J. Warner, S. Khanna, G. Seguin, and G. Brassard, "A 60-channel superconductive input multiplexer integrated with pulse-tube cryocoolers," *IEEE Trans. Microwave Theory Tech.*, vol. 48, pp. 1171–1180, July 2000.

[4] D. Zhang, G. C. Liang, C. F. Shih, Z. H. Lu, and M. E. Johansson, "A 19-pole cellular bandpass filter using 75-mm-diameter high-temperature superconducting thin films," *IEEE Microwave Guided Wave Lett.*, vol. 5, pp. 405–407, Nov. 1995.

[5] M. J. Lancaster, F. Huang, A. Porch, B. Avenhaus, J. S. Hong, and D. Hung, "Miniature superconducting filters," *IEEE Trans. Microwave Theory Tech.*, vol. 44, pp. 1339–1346, July 1996.

[6] J. S. Hong and M. J. Lancaster, "Cross-coupled microstrip hairpin-resonator filters," *IEEE Trans. Microwave Theory Tech.*, vol. 46, pp. 118–122, Jan. 1998.

[7] J. S. Hong, M. J. Lancaster, D. Jedamzik, and R. B. Greed, "On the development of superconducting microstrip filters for mobile communications applications," *IEEE Trans. Microwave Theory Tech.*, vol. 47, pp. 1656–1663, Sept. 1999.

[8] K. F. Raihn, R. Alvarez, J. Costa, and G. L. Hey-Shipton, "Highly selective HTS band pass filter with multiple resonator cross-couplings," in *IEEE MTT-S Int. Microwave Symp. Dig.*, June 2000, pp. 661–664.

[9] K. C. Gupta, R. Garg, I. Bahl, and P. Bhartia, *Microstrip Lines and Slotlines*, 2nd ed. Boston, MA: Artech House, 1996, p. 103.

[10] A. E. Atia and A. E. William, "Narrow bandpass waveguide filters," *IEEE Trans. Microwave Theory Tech.*, vol. MTT-20, pp. 258–265, Apr. 1972.

[11] R. J. Cameron and J. D. Rhode, "Asymmetric realization for dual-mode bandpass filters," *IEEE Trans. Microwave Theory Tech.*, vol. MTT-29, pp. 51–58, Jan. 1981.

[12] R. Levy, "Direct synthesis of cascaded quadruplet (CQ) filters," *IEEE Trans. Microwave Theory Tech.*, vol. 43, pp. 2940–2945, Dec. 1995.

[13] J. S. Hong and M. J. Lancaster, *Microstrip Filters for RF/Microwave Applications*.   New York: Wiley, 2001, ch. 8.

[14] K. A. Zaki, private communication, Mar. 2002.

[15] B. Ute, S. Rieder-Zecha, and H. Kinder, "Continuous $YBa_2Cu_3O_{7-\delta}$ film deposition by optically controlled reactive thermal co-evaporation," *IEEE Trans. Applied Superconduct.*, vol. 7, pp. 1181–1184, June 1997.

[16] H. R. Yi, S. K. Remillard, and A. Abdelmonem, "A superconducting thin film filter of very high wide-band rejection," in *IEEE MTT-S Int. Microwave Symp. Dig.*, June 2003, pp. 1893–1896.

[17] S. K. Remillard, H. R. Yi, and A. Abdelmonem, "Three-tone intermodulation distortion generated by superconducting bandpass filters," *IEEE Trans. Appl. Superconduct.*, vol. 13, pp. 3797–3802, Sept. 2003.

H. R. Yi (SM'02) received the B.S. degree in physics from the University of Science and Technology of China, Hefei, China, in 1988, the M.S. degree in physics from the Chinese Academy of Sciences, Beijing, China, in 1991, and the Ph.D. degree in physics from the Chalmers University of Technology, Göteborg, Sweden, in 1996.

From March 1991 to February 1993, he was a Staff Member with the Institute of Physics, Chinese Academy of Sciences. From March 1993 to November 1996, he was a Research Assistant with the Department of Physics, Chalmers University of Technology. From December 1996 to August 1998, he was a Post-Doctoral Fellow and from September 1998 to October 2001, he was a scientific employee with the Research Center of Jülich, Jülich, Germany. From November 2001 to January 2003, he was a Senior RF Engineer with ISCO International, Mount Prospect, IL. In January 2003, he joined Netcom Inc., Wheeling, IL, as a Principal Engineer. His fields of interest are the design and realization of high-Tc superconducting thin-film filters, dielectric-resonator filters, and tunable filters. His previous research fields include high-Tc thin films, Josephson junctions, and superconducting quantum interference devices (SQUIDs). He has authored or coauthored over 60 papers. He holds five patents with two patents pending.

Stephen K. Remillard (M'91) was born in Galesburg, IL, in 1966. He received the B.S. degree (with honors) in physics from Calvin College, Grand Rapids, MI, in 1988, and the M.S. and Ph.D. degrees in physics from the College of William and Mary, Williamsburg, VA, in 1990 and 1993, respectively.

A portion of his doctoral research was performed at the Naval Research Laboratory, where he studied the microwave properties of high temperature superconductors. He also researched the fabrication of HTS materials at BUGH Wuppertal, Wuppertal, Germany, and at the Los Alamos National Laboratory, Los Alamos, NM. Upon completion of his doctoral studies, he joined the Illinois Superconductor Corporation (now ISCO International), Mount Prospect, IL, where he investigated ways to improve the power handling of HTS RF filters. In 1998, he became the Director of Engineering with ISCO International, where he led the development of HTS filter systems. He is currently with Agile Devices Inc., Evanston, IL.

Amr Abdelmonem (M'92–SM'00) received the B.Sc. and M.S. degrees in electrical engineering from Ain-Shams University, Cairo, Egypt, in 1987 and 1990, respectively, and the Ph.D. degree in electrical engineering from the University of Maryland at College Park, in 1994.

In January 1995, he joined ISCO International, Mount Prospect, IL, where he is currently the Chief Executive Officer (CEO). He has directed the design and implementation of the first successful field trial of a superconductor filter in a cellular base station. His primary responsibility is defining the optimal direction of the technology and strategic partnership efforts with major third-generation (3G) original equipment manufactures (OEM) wireless equipment providers. Prior to joining ISCO International, he held teaching positions with Ain-Shams University and the University of Maryland at College Park. The majority of his research has focused on superconducting technology, advanced filter design, semiconductor laser design and optical communication. He has authored or coauthored numerous papers for industry conferences and trade journals. He currently holds five HTS related patents and has several patents pending.